**Earthquake and Structures**, *Vol. 18, No. 1 (2020) 1-14*
DOI: https://doi.org/10.12989/eas.2020.18.1.014


# Seismic response of a highway bridge in case of vehicle-bridge dynamic interaction

Yildirim S. Erdogan*[1] and Necati F. Catbas[2]

[1]*Yildiz Technical University, Civil Engineering Department, Istanbul, Turkey*
[2]*Department of Civil, Environmental and Construction Engineering, University of Central Florida, Orlando, United States*

*(Received September 14, 2019, Revised December 3, 2019, Accepted December 18, 2019)*

**Abstract.** The vehicle-bridge interaction (VBI) analysis might be cumbersome and computationally expensive in bridge engineering due to the necessity of solving large number of coupled system of equations. However, VBI analysis can provide valuable insights into the dynamic behavior of highway bridges under specific loading conditions. Hence, this paper presents a numerical study on the dynamic behavior of a conventional highway bridge under strong near-field and far-field earthquake motions considering the VBI effects. A recursive substructuring method, which enables solving bridge and vehicle equations of motion separately and suitable to be adapted to general purpose finite element softwares, was used. A thorough analysis that provides valuable information about the effect of various traffic conditions, vehicle velocity, road roughness and effect of soil conditions under far-field and near-field strong earthquake motions has been presented. A real-life concrete highway bridge was chosen for numerical demonstrations. In addition, sprung mass models of vehicles consist of conventional truck and car models were created using physical and dynamic properties adopted from literature. Various scenarios, of which the results may help to highlight the different aspects of the dynamic response of concrete highway bridges under strong earthquakes, have been considered.

**Keywords:** vehicle-bridge interaction; recursive solution of coupled equation; far-field near-field earthquake motion; highway bridges; sprung-mass vehicle models

## 1. Introduction

Understanding the response of bridge structures under operational conditions is crucial for design considerations and structural safety. Specifically, bridge response may be complicated under different traffic conditions in case of vehicle-bridge interactions. Besides, it is well known that the strong earthquake motions may be destructive for improperly designed bridges. Recently, these two loading conditions can be considered together since it is very likely that an earthquake can strike a bridge when it is load by vehicle traffic. Especially, in crowded cities, this kind of situation, which might be catastrophic, can be encountered.

The vehicle-bridge interaction (VBI) problem has been widely discussed by researches and various numerical algorithms have been developed in this context. Zhang and Xia (2013) introduced an inter-system iteration method in order to solve coupled vehicle-bridge system of equations. By this method, two systems are solved iteratively and separately over the complete simulation time. Beside, time step iteration method in which the vehicle and bridge subsystems are solved simultaneously at each time step was used in (Jo *et al*. 2008). Three time integration algorithms, adequate for solving VBI problems were compared in Liu *et al*. (2014). Youcef *et al*. (2013) investigated the effect of rail irregularities on the dynamic response of train-bridge system via time integration of coupled system of equations. Explicit and implicit integration methods were used to solve the coupled equations of suspension type monorail system in Cai *et al*. (2019). The authors used a general purpose commercial FE program and compared the results with the experimental data. Zhou *et al*. (2017) investigated the coupled vehicle-bridge dynamics considering nonlinear support stiffness, mass ratio and excitation amplitude. They have shown that these parameters lead to complex dynamic behavior of the bridge. Recently, a VBI analysis, which includes the effect of debris flow impact on the dynamic response of bridge was carried using hybrid implicit-explicit time integration technique in Zhang *et al*. (2019). Another recent study that can be used to identify the road roughness based on vehicle-bridge interaction was proposed by Zhan *et al*. (2019) and demonstrated by numerical simulations. Wang *et al*. (2016a) introduced a recursive solution method in order to analyze a multi-span continuous bridge. The method is capable of solving VBI problems with complex bridge-vehicle systems and traffic conditions. The method was also applied to investigate the resonance conditions of cable-stayed bridges under vehicular loadings (Wang *et al.* 2016b). A state-of-the art review can be found in Zhai *et al*. (2019). Besides, a state-of-the-art review that summarizes the research directed towards the response of bridges in case of VBI together with the modal identification and the damage detection in bridges under moving vehicles was presented by Yang and Yang (2018).

Many authors have studied on the seismic response of bridge structures to assess the seismic safety and

*Corresponding author, Assistant Professor
E-mail: serhate@yildiz.edu.tr


http://www.techno-press.com/journals/eas&subpage=7
ISSN: 2092-7614 (Print), 2092-7622 (Online)

prospective damage mechanisms. Jiang *et al*. (2019) investigated the earthquake response of a scaled high-speed railway bridge experimentally. The effect of pounding between a skewed highway bridge and abutments during seismic excitation was studied by Chen *et al*. (2017). Nonlinearity in bridge columns, bearings and pile-soil interaction were included in their model. Another study that considers the post-earthquake damage of columns of a highway bridge was presented in Ge *et al*. (2019) and Farahani and Maalek (2017). The effect of earthquake motion characteristics on the response of an isolated bridge considering soil-structure interaction was presented in Neethu *et al*. (2017). Recently, the effect of near-fault and far-fault earthquake motions on civil engineering structures was studied by many authors (Güllü and Karabekmez 2017, Ansari *et al*. 2018, Uckan *et al*. 2018). Besides, a study that focuses on analyzing the seismic vulnerability of a highway bridge under pulse-like near-fault ground motions was presented in Han *et al*. (2017). The sensitivity of earthquake response of a stone arch bridge to near-field and far-field earthquake motions was investigated in Simos *et al*. (2018). It was found that the far-field earthquake motions are more destructive than near-field earthquake.

Although the studies that concern the dynamic behavior of bridges and VBI analysis separately, are vast, the studies that consider the VBI under strong earthquake motions are relatively rare. A recent study that investigates the nonlinear response of a bridge-vehicle interactive system under strong earthquakes can be found in Borjigin *et al*. (2018). They investigated the effect of moving vehicles on dynamic response of a three span highway bridge under strong earthquake motions. They assumed that the vehicles with identical properties moving on the same lane with constant velocity and time interval. In Kameshwar and Padgett (2018), seismic response of two span highway bridge was investigated considering VBI. They concluded that the presence of a vehicle influences the performance of bridge components. Similar conclusions have been made in Zhou *et al*. 2018, in which the response of a long-span bridge under earthquake and moving vehicle was numerically calculated. It was demonstrated that the combined effect of earthquake and traffic excitations cause larger dynamic response compared to only earthquake or traffic excitations. In addition, the analysis of three span concrete highway bridge showed that the parameters such as number of vehicles, their speed and relative distance between them, greatly affect the dynamic response of bridge in case of VBI (Paraskeva *et al*. 2017). In Li and Conte (2016), the seismic response of a bridge was investigated considering soil-structure and track-structure interactions. However, the dynamic interaction of train-bridge was not considered in this study. A realistic simulation model that can be used to investigate the derailment conditions of a train moving on a bridge during was presented in Zeng and Dimitrakopoulos (2018).

Considering the fact that the earthquakes can strike bridges in crowded cities when they are loaded with complex traffic conditions, the dynamic response of a highway bridge under strong earthquake motions considering VBI was investigated in this study. A recursive substructuring method has been adopted for solving VBI equations. By this way, the VBI equations were uncoupled and solved separately using advanced commercial finite element software ANSYS, which does not have intrinsic features to solve the coupled equation of motions of VBI problem. A macro was developed by its parametric design language capability. The adopted method is generic and can be applied VBI problems including any nonlinearity in both bridge and vehicle substructures. In this study, three dimensional transient linear time history analysis was carried out to study the effect of vehicle velocity, traffic conditions, road roughness and near-field and far-field earthquake motions. Soil-structure interaction effect was also investigated under strong earthquake motions considering the VBI using the direct approach. Three dimensional sprung-mass models of representative car and truck vehicles were created. In order to create a random traffic condition in total of eight vehicle models were derived from the representative vehicle models. A real-life highway bridge with measured dynamic properties were calibrated and used throughout the numerical analysis. The results showed that the seismic response of the bridge can be greatly affected by vehicle velocity, traffic conditions and SSI. A resonance was also observed for specific vehicle velocity values.

## 2. The recursive approach for the inclusion of VBI effects in dynamic analysis under earthquake loads

An approach similar to the one proposed by Wang *et al*. (2016a) was used to include the VBI effects in the dynamic response analysis of a highway bridge under seismic actions. The method is generic and the effects of other environmental loads such as wind can also be considered. The method is summarized as follows:

1. step: An initial static analysis for the vehicles is conducted under gravity loads using Eq. (1).

$$\boldsymbol{K_v u_{vg}} = \boldsymbol{r M_v} g \tag{1}$$

Where, $\boldsymbol{K_v}$ and $\boldsymbol{M_v}$, are stiffness and mass matrices of the vehicle model, $\boldsymbol{u_{vg}}$ is the displacement vector and $\boldsymbol{r}$ is a vector, in which its all elements comprise of 1s, respectively. The degree of freedoms (*dof*s) that are to be in contact with the bridge deck are assumed to be fully constrained. If required the static analysis can also be carried out for the bridge substructure.

2. step: The reaction forces at the supports of vehicles (e.g., reaction forces between tires and ground) calculated from Eq. (1) together with any external loads such as earthquake loads $\boldsymbol{f_{eq}}$ are applied to the bridge substructure. Then, the equation of motion of bridge substructure given in Eq. (2) is obtained.

$$\boldsymbol{M_b \ddot{u}_b} + \boldsymbol{C_b \dot{u}_b} + \boldsymbol{K_b}\, \boldsymbol{u_b} = \mathbf{r}_{cv} + \boldsymbol{f_{eq}} \tag{2}$$

Where, $\boldsymbol{M_b}$, $\boldsymbol{C_b}$, $\boldsymbol{K_b}$ are the mass, damping and stiffness matrices of the bridge substructure. The force vector $\mathbf{r}_{cv}$ consists of $n$ x *dofn* number of nodal forces ($n$ is the number of forces in the domain of bridge deck, $dofn$ is number of *dof* of the corresponding finite element), which corresponds to forces that are applied to the nodes of the corresponding finite elements of bridge deck at any time $t$.

The *j*th contact force $r_{vs,j}$ is distributed along the *dofs* of corresponding bridge finite element by the use of shape functions (Eq. (4)). Where $N_{k,i}$ is the shape function of the *k*th bridge element corresponding to *i*th *dof*. The elements of contact force vector $\boldsymbol{r_{vs}}$ that are located inside the domain of bridge deck at time $t_s$ are nonzero as given in Eq. (3), where $t_j$ indicates the entry time of the axle to the bridge, $r_{v,j}$ is the *j*th reaction force calculated at the corresponding vehicle support, $v$ is the speed of axle, $\delta$ and $H$ are the Dirac delta and unit step function, respectively.

The Eq. (2) can be solved for bridge displacements $\boldsymbol{u_b}$ by integrating between $t_s$ and $t_{s+1}$ using any time integration method such as Newmark method using initial conditions and stress state at time $t_s$. The time interval $\Delta t_s = t_{s+1}$-$t_s$ should be small enough due to accuracy issues as discussed at the end of this section.

$$r_{vs,j}(x,t) = r_{v,j}\ \delta[x - v(t - t_j)][H(t - t_j) - H(t - t_j - \Delta t_s)] \tag{3}$$

$$r_{cv,i} = r_{vs,j} N_{k,i} \tag{4}$$

In addition to the equation of motion of the bridge substructure, equation of motion of vehicles given in Eq. (5) can be solved, separately in step 2. In this case Eqs. (5)-(6) are integrated between $t_s$ and $t_{s+1}$ using initial conditions and stress state at time $t_s$. Here, $u_v^c$ is the displacements at the supports of the vehicles that are in contact with the bride deck elements and $u_b^c$ is the bridge displacement calculated from Eq. (2) corresponding to these displacements *dof*s of the vehicle. After solving Eqs. (5) and (6), the reaction force vector $\boldsymbol{r_v}$ calculated at the supports are used to calculate $\boldsymbol{r_{vs}}$ and $\boldsymbol{r_{cv}}$, which are to be used to integrate Eq. (2) in between $t_{s+1}$ and $t_{s+2}$. Hence, a recursive analysis, which enables to solve the equations of motions of both bridge substructure and vehicles, separately.

Obviously, the solution of Eq. (5) is carried out by imposing the bridge displacements to the support of vehicles. The imposed bridge displacements are obtained from the solution of Eq. (2) alone (e.g., not from the coupled solution of Eqs. (2) and (5)). Hence, the change in the position of a vehicle axle that is in contact with the bridge deck should not be too large between two consecutive time steps. Otherwise, the error in the results obtained from the presented analysis can be large in comparison to the solution of coupled system of equations.

$$\begin{gathered}\boldsymbol{M_v \ddot{u}_v} + \boldsymbol{C_v \dot{u}_v} + \boldsymbol{K_v u_v} = \boldsymbol{r M_v} g \\ \text{s.t. } \boldsymbol{u_v^c}(t = t_{s+1}) = \boldsymbol{u_b^c}(t = t_{s+1})\end{gathered} \tag{5}$$

The position of any axle on the bridge deck can be arbitrary and does not have to be coincide with a node of finite element. Hence, the displacement of the bridge at the *j*th contact position can be calculated using the shape functions of the finite element used to discretize the deck of the bridge as given in Eq. (6).

$$u_{b,j}^c = \sum_{i=1}^{dofn} N_{k,i}(\xi_c, \eta_c) u_{k,i} \tag{6}$$

Commonly, the shape function of the *k*th element corresponds to *i*th *dof* $N_{k,i}(\xi,\eta)$ are given as functions of local coordinate variables $\xi$ and $\eta$. Thus, the position of *j*th axle should be calculated in terms of local coordinates $\xi_c$ and $\eta_c$ given the global coordinates $x_{c,j}$ and $y_{c,j}$ of the axle at any time *t* and the coordinates $x_{k,1}, y_{k,1}$ of the nodes of the *k*th element. To do so, 2×2 nonlinear system of equations given in Eq. (7) has to be solved for $\xi_c$ and $\eta_c$ using Newton-Rapson method in order to calculate the value of $N_{k,i}(\xi_c, \eta_c)$. It is noted that the solution is converged in few iterations (2-3 iterations). Hence, the computational burden in the calculation of the position coordinates of axle due to Newton Raphson iterations is not too much. Additionally, the road roughness can simply be considered by adding the bridge deck roughness value to the bridge displacement at the corresponding *dof* e.g. $u_k + r(x_k)$ (Wang *et al.* 2016).

$$\begin{bmatrix} N_1(\xi_c,\eta_c) & \dots & N_{dofn}(\xi_c,\eta_c) & 0 \\ 0 & N_1(\xi_c,\eta_c) & \dots & N_{dofn}(\xi_c,\eta_c) \end{bmatrix} \times \begin{bmatrix} x_{k,1} \\ \vdots \\ x_{k,dofn} \\ y_{k,1} \\ \vdots \\ y_{k,dofn} \end{bmatrix} = \begin{bmatrix} x_{c,j} \\ y_{c,j} \end{bmatrix} \tag{7}$$

As it was shown that the equations of motion of the bridge and vehicle substructures can be considered uncoupled and may be solved, separately. Hence, the method can be adapted to advanced commercial FE packages such as ANSYS and ABAQUS. The parametric programming language capability of these FE programs is appropriate for this purpose. In this study ANSYS FE package and its macros have been used to develop and execute the method. By doing this, it is also possible to include nonlinearities in both vehicles and bridge substructures if it is of concern. The flowchart of the recursive approach is given in Fig. 1.

In order to compare the accuracy of the adopted method, the results from the recursive analysis were compared with the analytical results from a two *dof*s vehicle moving along a simply supported beam. Comparison was made between the analytical solution provided by Yang *et al*. (2019) and the numerical results from the adopted method for different time step sizes. However, same substep size (0.005) was chosen for each time integration between consecutive time steps (e.g., between $t_s$ and $t_{s+1}$). It is obvious in Figure 2 that the analytical and the numerical results are very close for small step sizes ($d_t = 0.01$). The differences increases for higher step sizes, yet, these differences are not too high although the chosen step sizes ($d_t = 0.08$ and $d_t = 0.15$) are very large for a transient analysis. It can be mentioned that the accuracy of the adopted approach is appropriate for the numerical VBI analysis.

## 3. Finite element model of the highway bridge and model calibration

The Bridge 2028 in Cayey, Puerto Rico, which was studied by Catbas *et al*. (2006) and Borgo *et al*. (2006) was

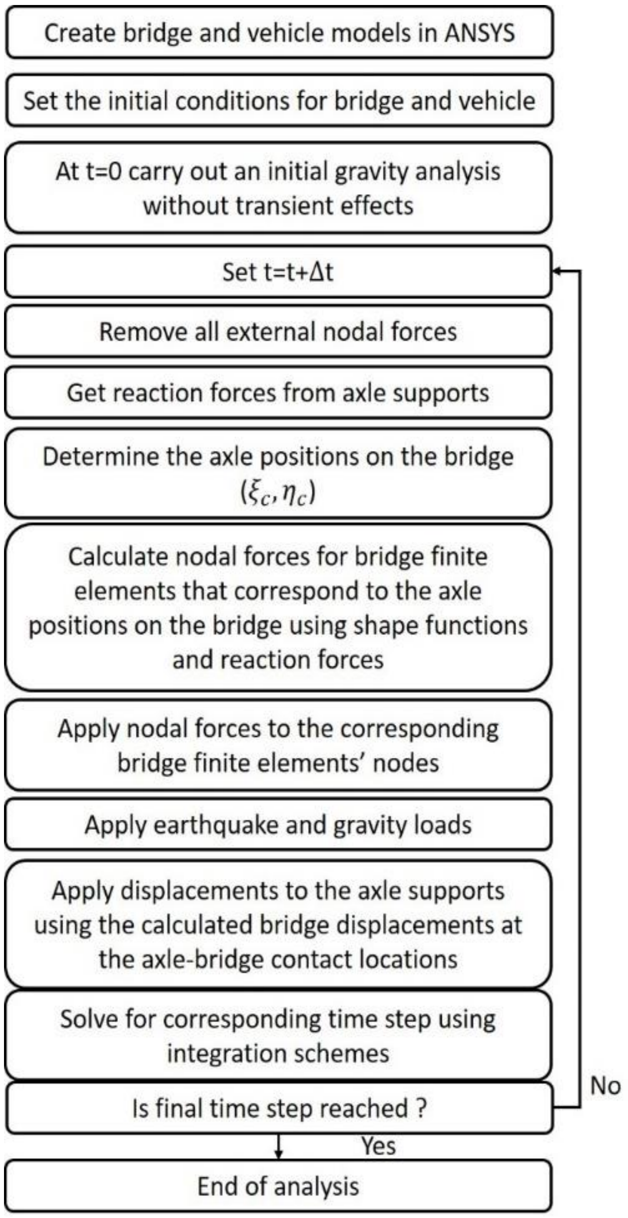


Fig. 1 Flowchart for the recursive VBI analysis under earthquake motion

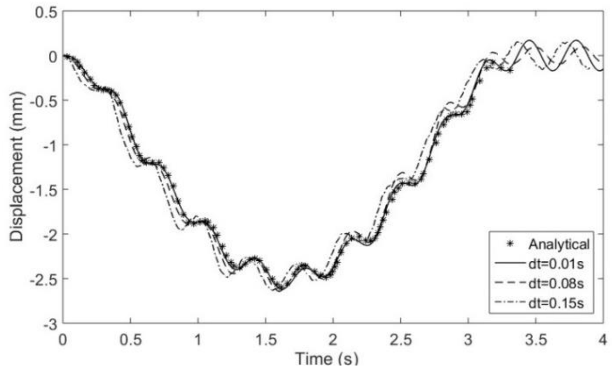


Fig. 2 Comparison of the accuracy of the method for various time step size for two axle vehicle moving on simply supported beam

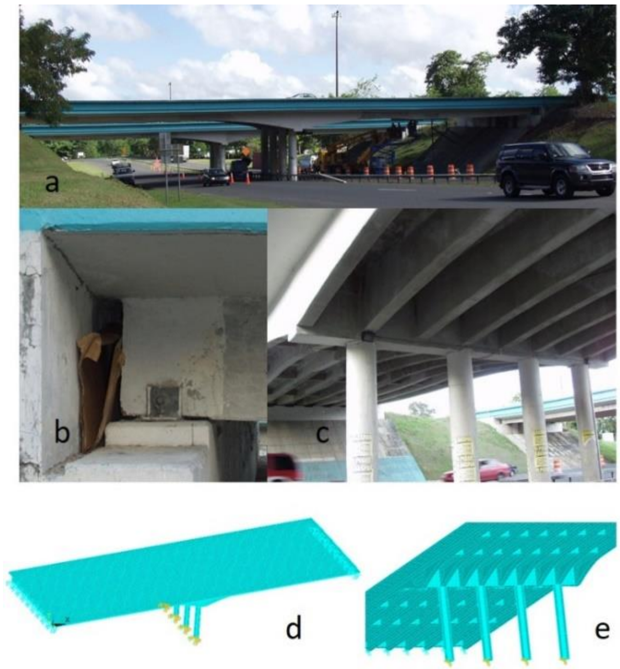


Fig. 3 Bridge 2028 a) side view, b) girder-abutment connection c) bottom view d) FE model-top view e) FE model-bottom view

adopted as the benchmark bridge structure in this study. The bridge is a two span conventional highway bridge composed of concrete T beams with 25m length. The bridge has three traffic lanes. The geometric and material properties of bridge can be found in Catbas *et al*. (2006). The bridge and its corresponding FE model were given in Fig. 3. The bridge girder-abutment connections can be assumed to be pin constraint as seen in Fig. 3(b). The static and the ambient vibration testing were carried out on the bridge. The frequency domain decomposition method (Brincker *et al*. 2007) was used to extract the natural frequencies and the modal shapes from the acceleration time history measurements. The acceleration data obtained from the mid-span of the side girders were used in modal extraction. Singular value diagram is presented in Fig. 4, while the numerical and the experimental modal shapes are given in Fig. 5, comparatively. The initial FE model was calibrated by experimentally measured natural frequencies using sensitivity-based FE model updating technique (Mottershead *et al*. 2011, Reynders *et al*. 2010). The bridge was divided into three subsection and different Young's modulus values were assigned and calibrated using first four natural frequencies.

## 4. Numerical models of Vehicles and Traffic conditions

Three dimensional sprung-mass models of vehicles have been created in order to simulate various traffic conditions. In total, eight different vehicle models have been created of which six of them were derived from two reference vehicle models. The first reference model is a standard car model and the second one is HS20-44 truck, which is commonly proposed by many codes for design purposes. The car and

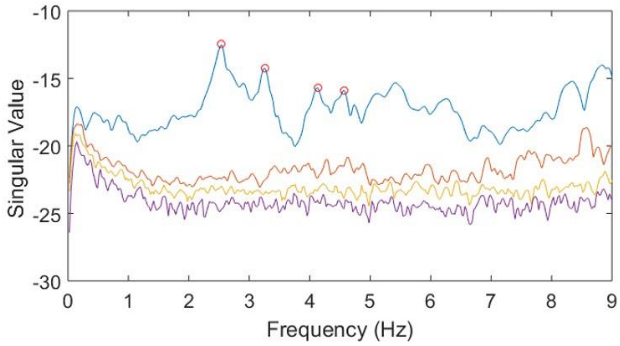


Fig. 4 Singular value diagram

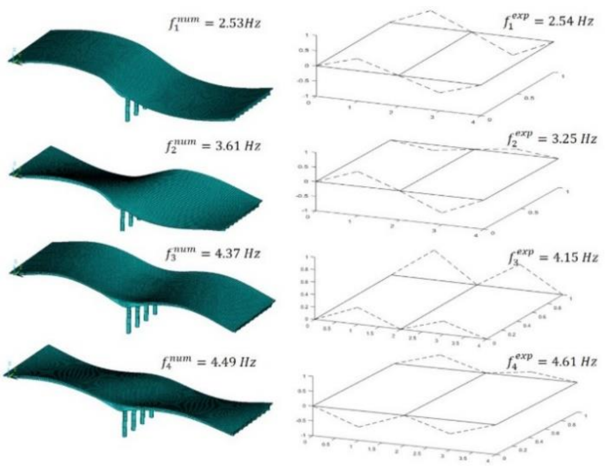


Fig. 5 Bridge 2028 numerical and experimental mode shapes. From top to bottom,first to fourth vibration modes

Table 1 Model parameters and dynamic properties of vehicle models

| Vehicle No | Body Mass (kg) | Axle suspension spring constant (N/m) | 1st mode frequency (Hz) | 2nd mode frequency (Hz) | 3rd mode frequency (Hz) |
|---|---|---|---|---|---|
| 1 | 26113 | 1969000 | 0.653 | 2.149 | 2.938 |
| 2 | 13000 | 1969000 | 0.653 | 2.748 | 3.164 |
| 3 | 24000 | 2369000 | 0.691 | 2.349 | 2.959 |
| 4 | 26113 | 1469000 | 0.591 | 1.955 | 2.913 |
| 5 | 1613 | 27278 | 0.820 | 1.043 | 1.149 |
| 6 | 1613 | 32278 | 0.859 | 1.068 | 1.210 |
| 7 | 2100 | 29278 | 0.836 | 1.025 | 1.059 |
| 8 | 1200 | 27278 | 1.820 | 1.043 | 1.332 |

the truck models were created based on the model properties published in Kim *et al*. (2002) and Harris *et al*. (2007), respectively. The other vehicle models are variant of these reference models created by changing the mass and stiffness properties of body and suspension system. The first three vibration modes of the reference car and the truck models are given in Figure 6. As seen, the first three modes of the car model are roll mode, pitch mode and the bounce mode, respectively. For the truck, the first three modes are rear wheel twisting mode, bounce and pitch mode, respectively. It is also noted that the stiffness of the vehicles

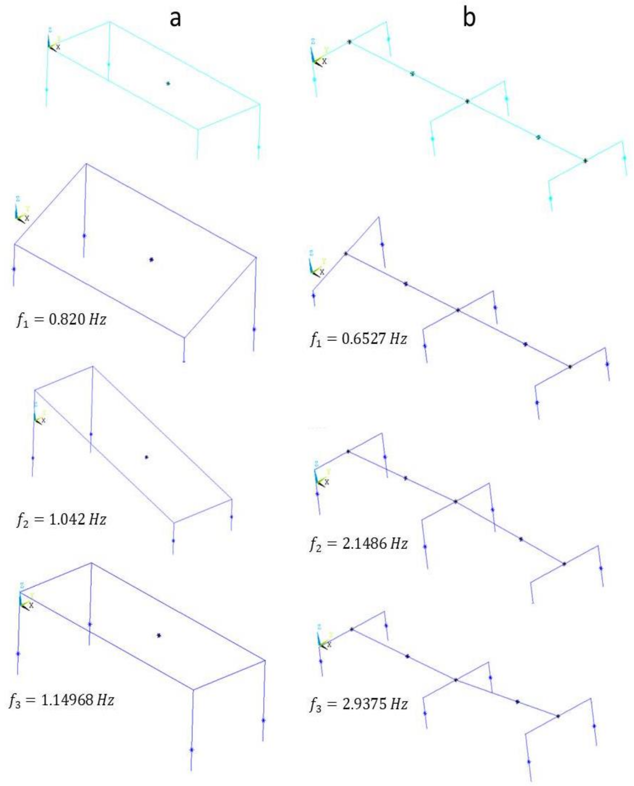


Fig. 6 Mesh grid of topographic model

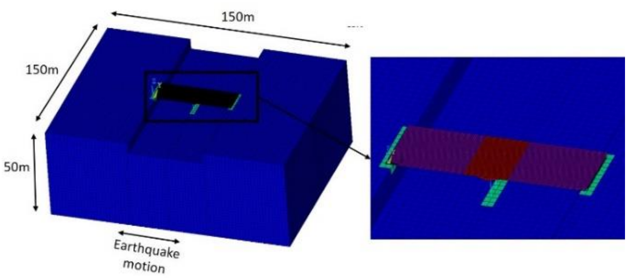


Fig. 7 FE model for SSI analysis using direct method

in the lateral and the longitudinal directions are too high compared to vertical stiffness. The model parameters and the modal properties of all vehicle types used in the analysis are presented in Table 1.

Three traffic conditions were considered in the numerical analysis. The first one consists of only reference car model while the second traffic conditions includes only reference truck model. In these two cases, the vehicles in different lanes were assumed to move side by side. Although this kind of traffic flow may not be observed in real life, these conditions can be considered as the extreme cases. The last traffic condition is a random traffic condition. In this case, the vehicles moving on each lane were uniformly sampled from eight different vehicle models. The time of entry of vehicles to the corresponding lanes is also different. However, the time interval between consecutive vehicles are assumed to be same.

## 5. Soil-structure interaction model

Table 2 Properties of the adopted earthquake ground motions

| Fault | Earthquake name | Station | PGA($m/s^2$) | | | PGV$m/s$ | | | PGV/PGA($s$) | | | Mw | Distance to Fault (km) |
|---|---|---|---|---|---|---|---|---|---|---|---|---|---|
| | | | N-S | E-W | U-D | N-S | E-W | U-D | N-S | E-W | U-D | | |
| Near-fault | 2010 Darfield | HORC& Horcn18-E | 2.64 | 2.80 | 4.77 | 0.63 | 0.41 | 0.37 | 0.24 | 0.15 | 0.07 | 7 | 7.29 |
| Far-fault | 2010 Darfield | FDCS & Fdcss81-W | 2.64 | 2.80 | 4.77 | 0.20 | 0.37 | 0.52 | 0.08 | 0.13 | 0.11 | 7 | 90.17 |
| Near-fault | Imperial Valley | Aeropuerto Mexicalli | 2.94 | 2.66 | 1.57 | 0.43 | 0.24 | 0.05 | 0.15 | 0.09 | 0.03 | 6.5 | 0.00 |
| Far-fault | Imperial Valley | Calipatria fire station | 2.94 | 2.66 | 1.57 | 0.23 | 0.23 | 0.09 | 0.08 | 0.08 | 0.05 | 6.5 | 23.17 |
| Near-fault | 1999 Kocaeli | Meteroloji istasyonu | 2.25 | 1.66 | 1.39 | 0.70 | 0.24 | 0.15 | 0.31 | 0.15 | 0.11 | 7.5 | 1.38 |
| Far-fault | 1999 Kocaeli | Bolu Göynük | 2.25 | 1.66 | 1.39 | 0.18 | 0.11 | 0.14 | 0.08 | 0.07 | 0.10 | 7.5 | 64.95 |

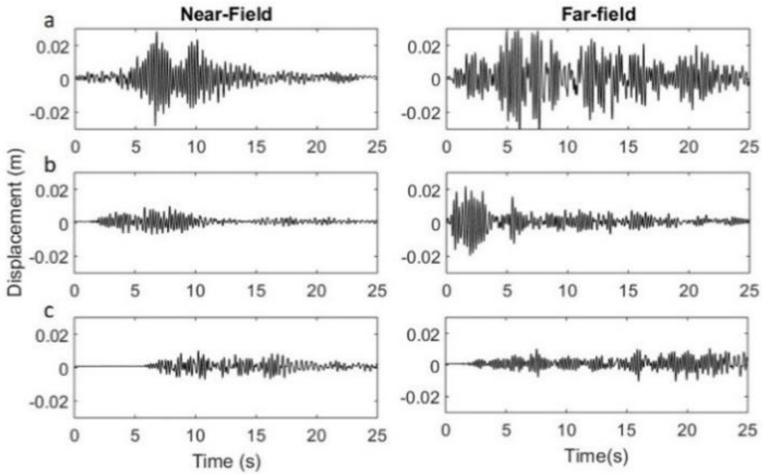


Fig. 8 Vertical displacement histories of the bridge in w/o vehicle case. a) Darfield b) Imperial Valley c) Kocaeli earthquake motion

A direct approach, which was used by Bolisetti *et al.* (2018), has been adopted for SSI analysis. In this method, a large 3D domain of soil is modelled and the radiating waves are dissipated through soil damping, which was taken as 5% in this study. The lateral boundary nodes located in the same elevation were constrained to move together in the lateral and horizontal directions to enable the elements of boundaries to move in pure share. It is also noted that this method is suitable for vertically propagating lateral and horizontal shear waves. Hence, the inclusion of vertical component of earthquake motion is not straightforward in this method. A concrete foundation with two meters wide and height is created between bridge columns, girders and the soil. Since there is no common approach in determining the dimensions of soil domain as to effectively radiate the shear waves, the dimensions have been chosen by trial and error. First a 50 m soil depth was chosen. Then, the earthquake motion was deconvolved to obtain the earthquake motion at bedrock to be used in the SSI analysis. If the acceleration response calculated at the boundary node of the soil in the SSI analysis matches the results from site response analysis, it can assumed that the waves are dissipated well enough. By doing so, the lateral dimension of soil was chosen as 150 m. The earthquake motion was applied to the base of the soil domain as displacement histories. The SSI model of the bridge is given in Fig. 7.

## 6. The selected earthquake motions

Three near-fault and far-fault earthquake motions have been adopted in the numerical analysis according to the criteria suggested by the previous studies Güllü and Karabekmez (2017), Zhang and Wang (2013). The selected near-fault strong earthquakes satisfy the following conditions: 1) velocity pulse duration larger than 1.0s 2) measurement distance to fault is less than 10 km 3) PGV/PGA is larger than 0.1s. Otherwise the earthquake motion is assumed to be a far-fault strong earthquake motion. The maximum acceleration values of near-fault and far-fault earthquake motions have been normalized so as to make them have the same PGA values. Table 2 summarizes the properties of adopted strong earthquake motions. The earthquake motions have been imposed to the supports of highway bridge in three orthogonal directions as displacement constraints. The N-S, E-W and U-D components have been applied in the longitudinal, the lateral and the vertical directions, respectively.

## 7. Numerical results

The influence of various parameters including vehicle velocity, road roughness, traffic flow, soil-structure interaction, far-field and near-field earthquake effects on the

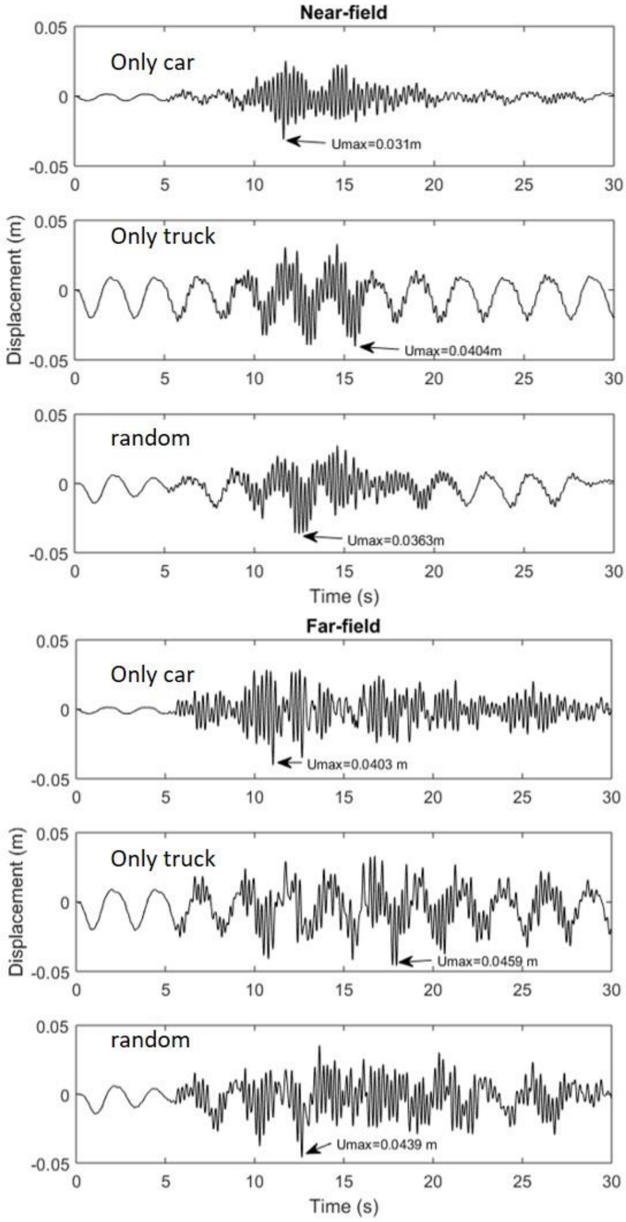


Fig. 9 Vertical displacement time histories under near-field and far-field Darfield earthquake motions

bridge dynamic response is investigated in this section. In Fig. 8, the displacement history of the bridge response measured at the mid-span of the side girders in the vertical direction is presented under far-field and near-field earthquake motions in the without vehicle case as reference results. The maximum response was achieved under Darfield earthquake motion. Besides, the displacement response under far-field earthquake motion is greater than the response obtained under near-field earthquake for each earthquake motions. This result is not surprising since it is known that the short period structures may experience larger response under far-field earthquake motions (Liao *et al*. 2004). Similar results were also reported by previous studies in Simos *et al*. (2017) and Güllü and Karabekmez (2017).

### *7.1 Comparison of various traffic conditions*

In most studies, it was assumed that the vehicles, which have same dynamic properties, are moving on the bridge side by side with a specific time interval. Hence, three traffic conditions mentioned in section 4 were first compared in order to see if there are considerable differences between the traffic conditions under strong far-field and near-field earthquake motions. The velocity and time delay between vehicles were taken as $20m/s$ and $2s$, respectively. The Darfield earthquake was used in the comparisons. The vertical displacement time histories for three traffic conditions were presented in Fig. 9. As expected, the highest displacement value is observed when the traffic flow is composed of only trucks. The maximum displacement value achieved in the random traffic condition is smaller than the only-truck traffic condition and higher than the only-car traffic condition. In addition, for each case, the displacements reach their maximum values at different times in each case. The time values at which the maximum displacement is achieved for only-car, only-truck and random cases are 11.6s, 15.6s and 12.49s, respectively. It should be mentioned that the maximum acceleration of the earthquake motion is around 15.7s. In the random traffic condition, the displacement values get smaller just after this time value due to different characteristics of the suspension systems of vehicles, which immediately damp out the vibrations. Besides, it was observed that the displacement amplitudes achieved under the far field earthquake motion are much higher compared to near field motion in all traffic conditions.

In addition, it was also checked if any vehicle loses its contact with the bridge deck. Hence, the vertical acceleration histories of vehicles' body were recorded. It was observed that only one vehicle's vertical acceleration value exceeded $9.81\,m/s^2$ in case of random traffic condition. In Fig. 10, vertical accelerations of this vehicle body together with the accelerations of vehicle bodies moving in front and behind of this vehicle are given. It was observed that the vehicle's vertical body acceleration reaches a value of $15\,m/s^2$, while the vertical acceleration of vehicles moving in the front and behind of this vehicle remain below $5\,m/s^2$. Except this instance no contact lost was observed.

### *7.2 Consideration of the effect of vehicle velocity and road roughness*

The effect of vehicle velocity on the earthquake response of the highway bridge was investigated under three far-field and near-field earthquake motions. Only displacement time-histories recorded at the mid-span of bridge side girder under Imperial Valley earthquake motion is presented in Fig. 11 for brevity. Similar displacement time histories were also obtained for Darfield and Kocaeli earthquakes. Interestingly, a resonance condition has been met for $v = 3\,m/s$ under both near-field and far-field earthquakes. Specifically, the resonance condition is much more severe under far-field earthquake. This resonance condition has also been observed for Darfield and Kocaeli earthquake motions. The Fourier spectrums given in Fig. 12

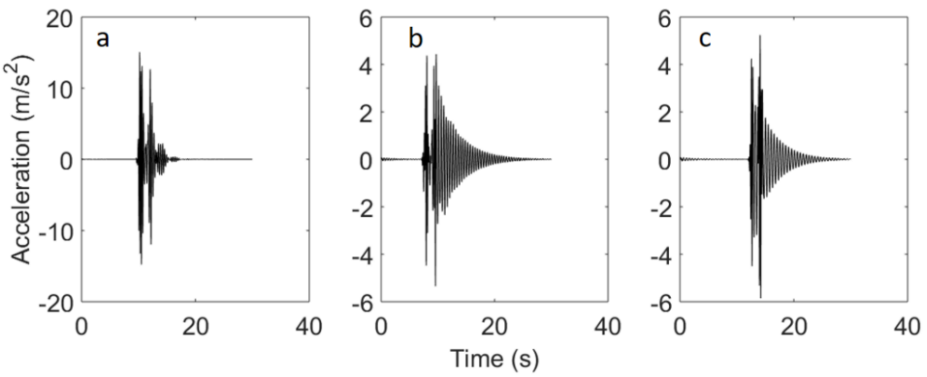


Fig. 10 Vertical acceleration of vehicle body (a) vehicle of which it acceleration value exceeds 1g (b) car moving front (c) car moving behind

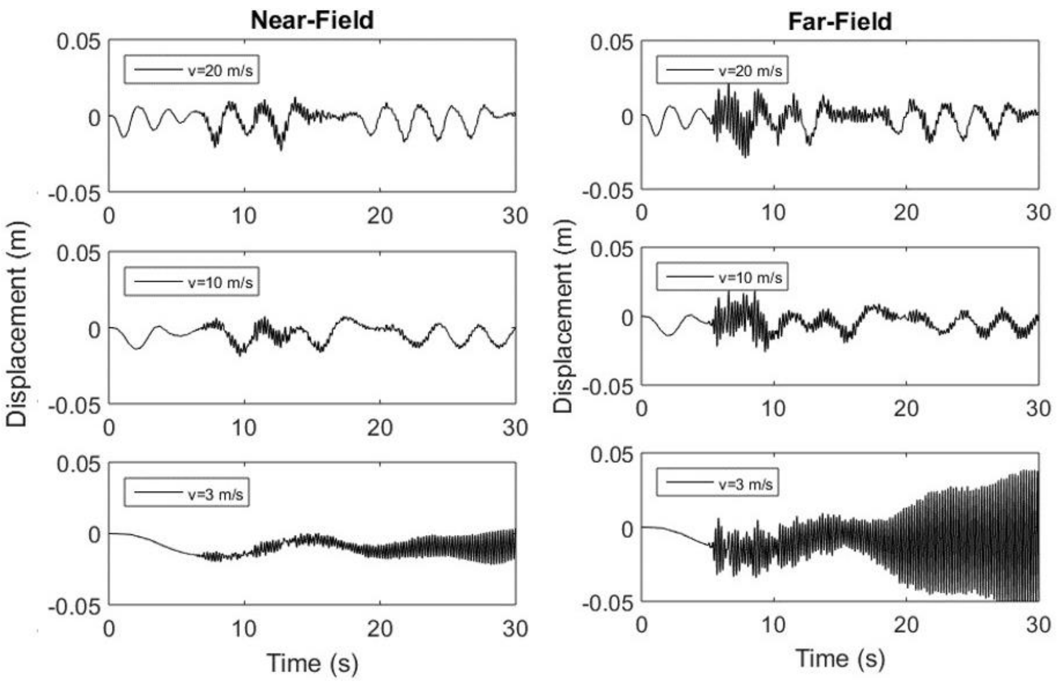


Fig. 11 Vertical displacement time histories under Imperial Valley earthquake motion for different vehicle velocities

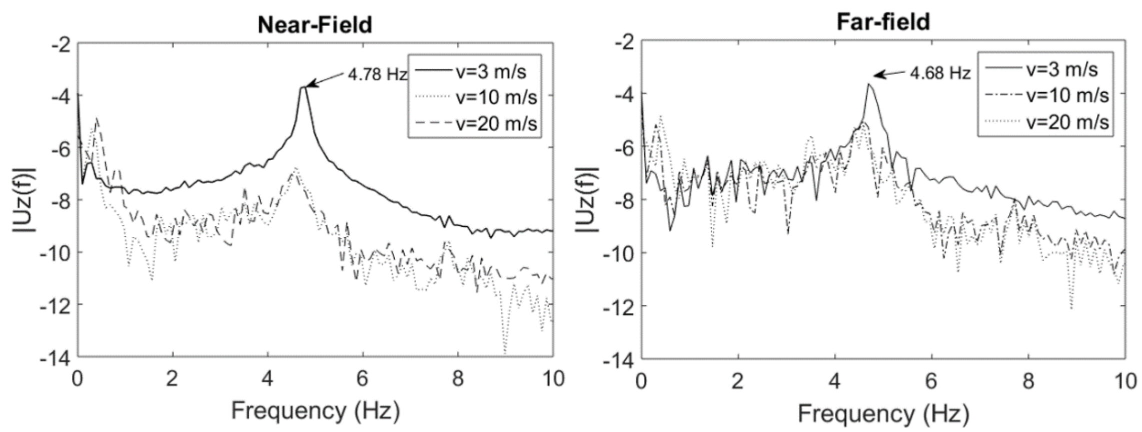


Fig. 12 Fourier spectrum of vertical displacement time histories

demonstrates that the resonance behavior of the bridge is related to the fourth vibration mode of the bridge. This mode corresponds to the second torsional mode. In Fig. 12, an apparent peak that corresponds to the fourth mode is observed for $v = 3\ m/s$ under both the far- field and the near-field earthquakes.

In Fig. 13, maximum vertical displacement and acceleration values recorded at the mid-span of the side

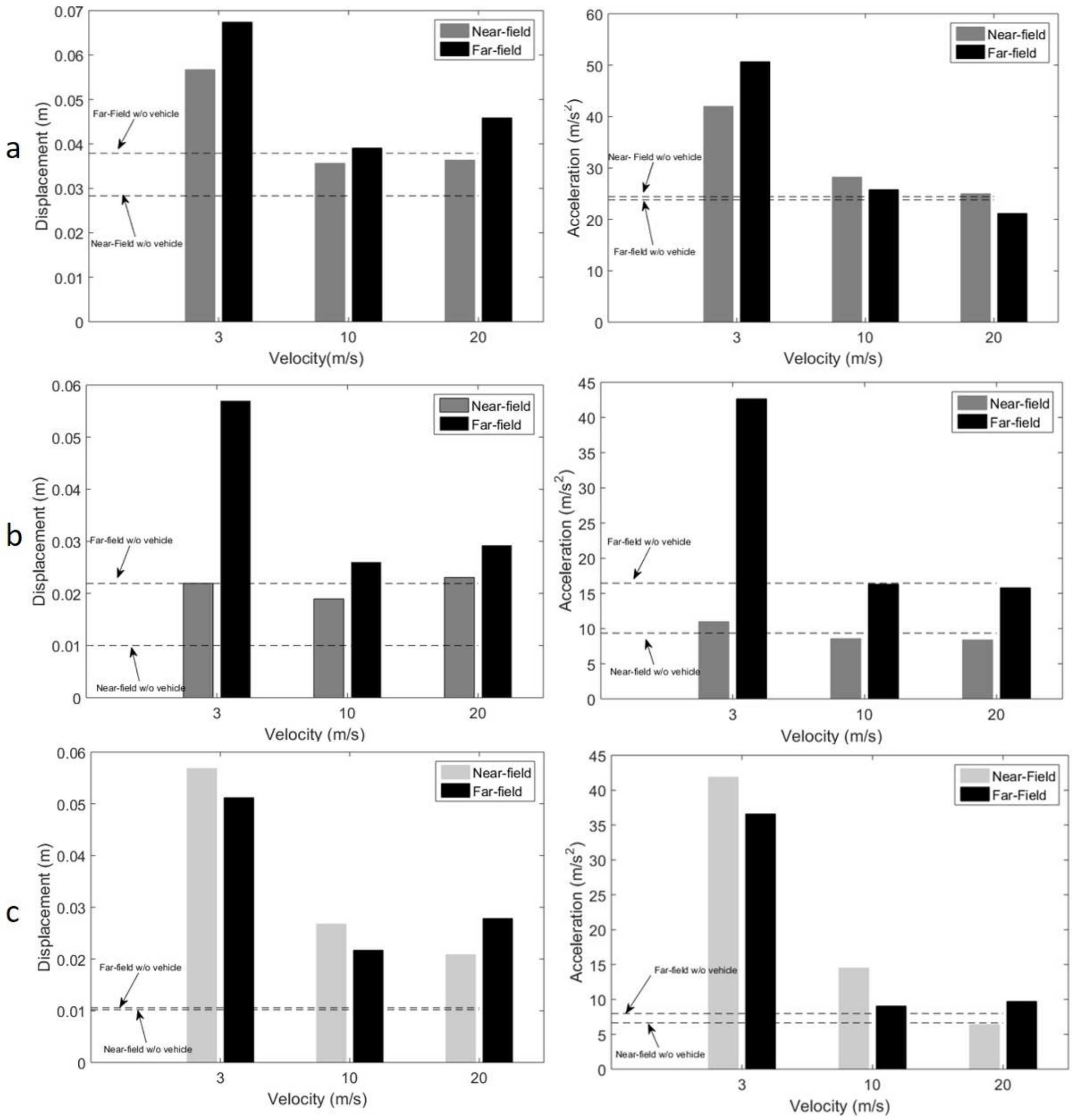


Fig. 13 Maximum recorded displacement and acceleration values. row (a) Darfield, row (b) Imperial Valley, row (c) Kocaeli earthquake

bridge girder are given for each earthquake motion. In general, both displacement and acceleration values obtained under far-field earthquakes are higher than the ones obtained under near-field earthquakes. However, the vehicle velocity greatly affects the response of the bridge during earthquake motion.

In Imperial Valley earthquake, lower velocities create higher differences in the response of bridge obtained under the effect of far-field and near-field earthquake. This is due to fact that the resonance condition that emerge for $v = 3\,m/s$ engender higher displacement values for far-field earthquake motion. However, there is no significant differences between the responses obtained for $v = 10\,m/s$ and $v = 20\,m/s$. The maximum response is slightly higher for $v = 20\,m/s$ compared to $v = 10\,m/s$ although mass of the bridge is higher when $v = 10\,m/s$ since there are more vehicles moving on the bridge during earthquake motion. This could be due to fact that the vehicle's suspension systems help to attenuate the dynamic response, which results in lower displacement values.

In all cases, the displacement response value of the bridge is higher compared to without vehicle case whatever the vehicle velocity is. However, this not true for maximum acceleration values. In some cases, it was observed that the maximum acceleration values obtained in with vehicle case are lower than without vehicle case due to damping arise from the vehicles' suspension mechanism. Besides, the far-field effect is lower than near-field effect for $v = 3\,m/s$ and $v = 10\,m/s$, while it is higher for $v = 20\,m/s$ in Kocaeli earthquake. Hence, it can be said that the dynamic response of the bridge is directly affected by the vehicle

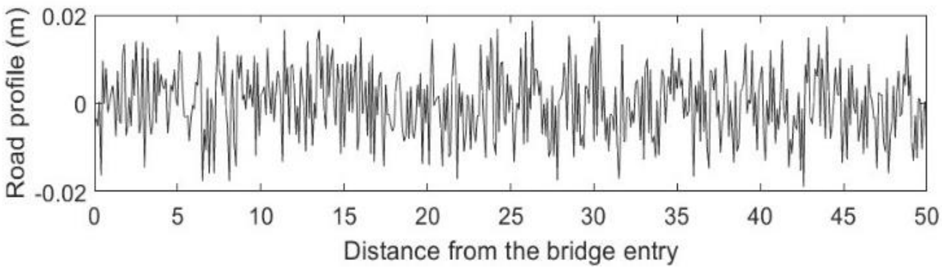


Fig. 14 Road roughness profile

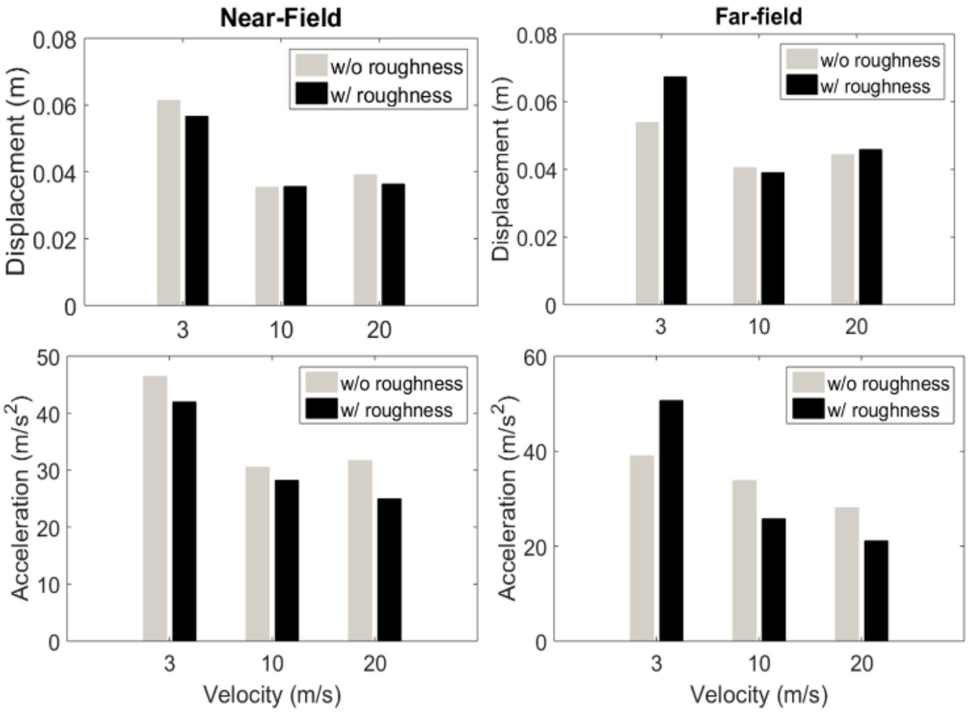


Fig. 15 Effect of road roughness on the dynamic response of bridge

velocity, the frequency content of the earthquake motion and their interaction. Due to the sophisticated interaction between bridge, vehicle and ground motion, an increasing or decreasing trend in maximum responses may not be necessarily observed. Similar results except the resonance condition were also presented by Paraskeva *et al*. (2017). It was stated that the vehicle speed might affect differently the seismic response of bridge. For instance, at a specific time, higher speed can either amplify or de-amplify the vertical displacement. However, as a common consequence it can be concluded that the vehicle velocity may significantly alter the seismic response of bridge.

It was also investigated that if the road roughness gives rise to a considerable increase in the bridge response under far-field and near-field earthquakes. The road roughness profile is given in Fig. 14. The maximum roughness value was chosen 2 cm, which is a reasonably high value for comparative purposes. Near-field and far-field Darfield earthquake motion was applied to highway bridge. The results given in Fig. 15 show that the there is no considerable difference in maximum displacements between with and without road roughness cases for velocities $v = 10\frac{m}{s}$ and $v = 20\frac{m}{s}$. However, the difference in displacements seems considerable for $v = 3\,m/s$ of which the resonance condition has met. This result is also comparable with the results from Paraskeva *et al*. (2017), of which they indicated that the effect road roughness is stronger for lower velocities. Besides, the acceleration values decrease when the road roughness is taken into account.

### *7.3 Effect of soil-structure interaction*

It is known that the velocity pulse of the near-fault ground motions is more significant compared to far-fault ground motions. Additionally, long period responses of near-fault ground motions is higher than far-field ground motions (Liao *et al*. 2004). Oppositely, the short period responses of far-field earthquakes may be more remarkable compared to near-fault earthquakes. It was shown that that the effect of far-field earthquakes are as great as the effect of near-field earthquake in some cases (Simos *et al*. 2017, Güllü and Karabekmez 2017). In this section, the SSI effects during VBI are investigated considering SSI effects rather than comparing far-field and near-field effects. The results were compared with the fixed base structure. Analysis were carried out for a soil medium with shear

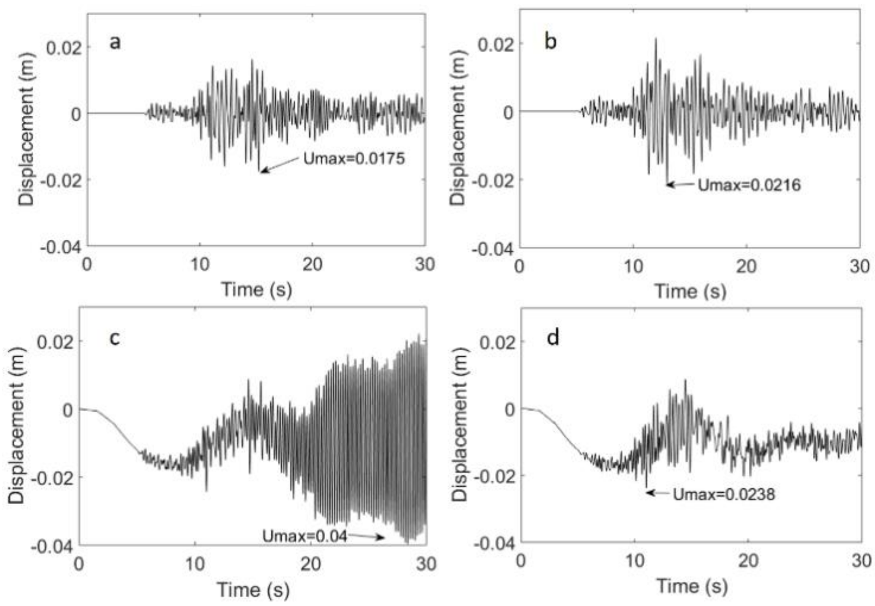


Fig. 16 Vertical displacement time histories (a) fixed base w/o vehicle (b) SSI w/o vehicle (c) fixed w/ vehicle (d) SSI w/ vehicle

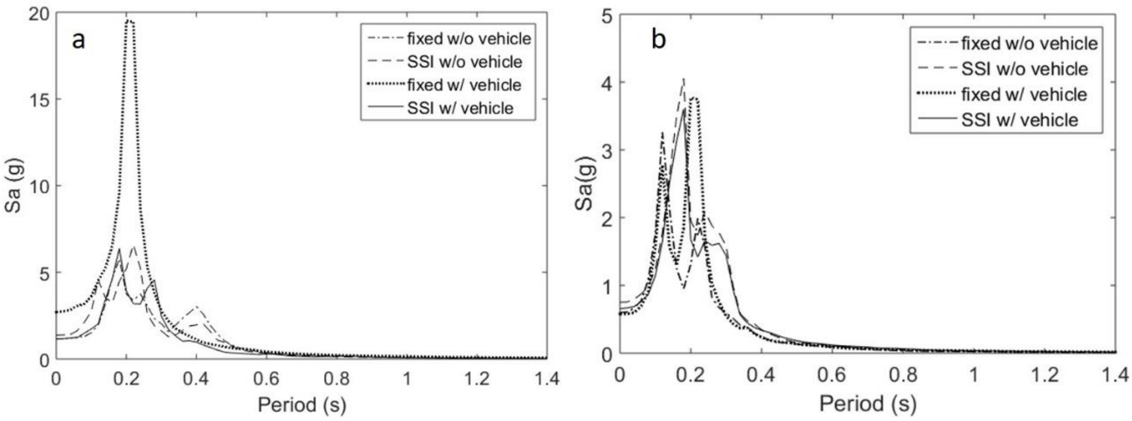


Fig. 17 Acceleration response spectra calculate at the mid-span of bridge girder (a) vertical component (b) lateral component of displacement response

velocity $V_s = 300\ m/s$, which corresponds to a soft soil made of sand or clay. The results were compared with the results obtained from fixed base conditions. The vehicle velocity $v = 3\ m/s$ was taken in all analysis carried out in this section. It should be stated that the vertical component of the earthquake motion was not considered since the adopted direct method is not suitable for that purpose. Hence, the presented displacement and acceleration values is smaller than the previously presented results. This also shows the remarkable effect of vertical component of earthquake motion on the bridge dynamic response.

The displacement time histories calculated at the mid-span of the side girder of the bridge for various cases are presented in Fig. 16. As expected the minimum displacement value was obtained in the fixed without vehicle case. The displacement value increased about 23% when SSI was included. However, the increase in vertical displacements obtained in case of SSI with vehicle is not remarkable (around 10%) compared to SSI without vehicle case. Besides, the resonance is observed in the fixed base condition when VBI is considered as observed previously (Fig. 16(c)). Interestingly, the resonance is not observed when SSI was included (Fig. 16(d)). This might be due to fact that the displacement waves are dissipated due to soft soil, which suppresses the resonance phenomenon.

The resonance effect is also obvious in the response spectra calculated from the vertical and the lateral displacement time histories given in Fig. 17. The single peak in the spectra of vertical displacement history is apparent in case of fixed base condition with VBI effects. In other cases, several peaks are observed for different periods. However, maximum spectral values of different cases do not differ significantly. Besides, resonance is not observed in the response spectra of lateral displacement histories. Additionally, lateral spectral values are considerably smaller than the spectral values of vertical displacement histories. The minimum spectral value is obtained for fixed base without vehicle case, while the maximum is observed in the SSI without vehicle case. It can also be said that the

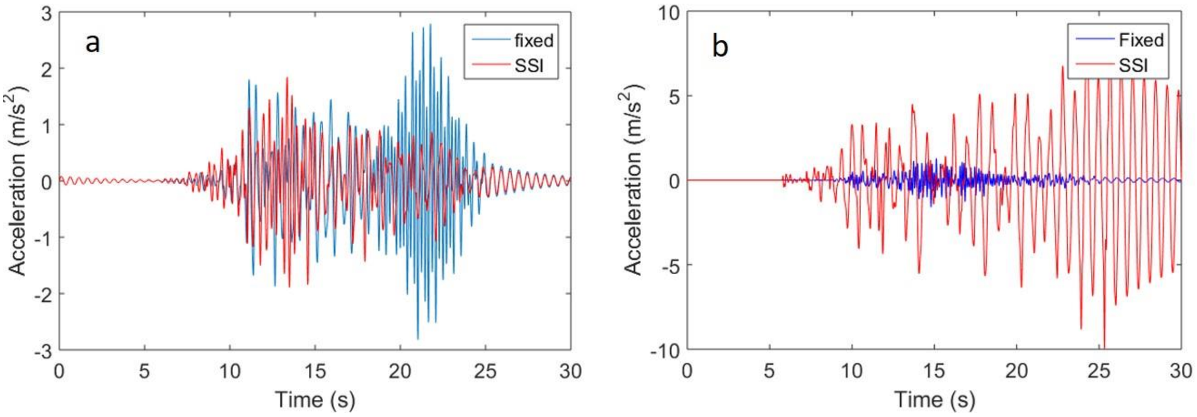


Fig. 18 Acceleration time history of vehicle body moving on the bridge when the ground motion reaches its maximum value (a) vertical component (b) lateral component of acceleration response

SSI with vehicle for soft soil does not engender a considerable effect compared to SSI without vehicle case. In other words, the vehicle-bridge interaction effect is insignificant when SSI is considered while it is significant when fixed based conditions are assumed as previously demonstrated. On the other hand, the acceleration response of the body of the vehicles moving on the bridge when the earthquake motion reaches its maximum acceleration is given in Fig. 18. It is observed that the vertical body acceleration diminishes after it reaches its maximum value in case of SSI. However, the acceleration reaches another peak in case of fixed base conditions. In both cases, the maximum accelerations are below $3m/s^2$, which indicates that the vehicle does not lose its contact between the bridge. Nevertheless, the lateral acceleration is excessive when SSI is considered. The maximum acceleration reaches about $9\,m/s^2$, which may cause the vehicle to overturn. As a result, the bridge maximum displacement response is not considerably affected by VBI in soft soil conditions, while the vehicle safety is of concern.

## 8. Conclusions

In this study, dynamic response of a real-life highway bridge was investigated under strong earthquake motions considering vehicle-bridge interaction (VBI). The bridge was first calibrated using experimental data obtained from in-situ dynamic tests. The effect of near-field and far-field earthquake motions together with effect of vehicle velocity, road roughness and soil-structure interactions (SSI) on the seismic response of the bridge were studied. A recursive substructuring method, which enables solving equations of motions of the bridge and the vehicle substructures separately was used for this purpose. The approach was coded and executed using ANSYS parametric design language and its accuracy was demonstrated.

The thorough numerical analysis results revealed many aspects of the seismic response of the bridge, which is to be notable for design purposes and bridge safety assessment. The traffic conditions, vehicle velocity and soil-structure interaction alter the dynamic response of bridge considerable. Following conclusions can be made from the results of the numerical analysis:

- It was revealed that the difference in displacement response with and without vehicle case is remarkable as it was also demonstrated by previous studies. The choice of traffic condition for realistic analysis is also necessary. The result may be conservative if the traffic is composed of all-truck, while the responses can be underestimated adopting all vehicles in traffic as standard car models. Besides, random traffic condition seems reasonable.
- No apparent trend was observed in the displacement and acceleration responses of vehicles for varying vehicle velocity. However, resonance was observed for vehicle velocity $v = 3m/s$. As it is well known, the resonance phenomenon, which depends on many parameters, is sophisticated and needs further investigation.
- Far-field earthquake motions in with vehicle case were found to be more significant and increases bridge response with respect to without vehicle case. This is not surprising since it is known that the short period response of far-field earthquakes can be higher compared to near-fault earthquakes. However, acceleration responses do not increase considerably, which may be damped out due to vehicle suspension system.
- When SSI in a soft soil medium is considered, the bridge response greatly increases compared to fixed base conditions without vehicle case. However, this increase is not remarkable when VBI is included. Interestingly, no resonance was observed in SSI with vehicle case as opposed to fixed base condition. It seems like the soft soil conditions compresses the resonance conditions.
- In case of SSI, the vertical accelerations of vehicles do not exceed the safety limit, while the lateral accelerations reach very high values. Thus, it can be concluded that the SSI effects introduces vehicle safety issues.

## References

Ansari, M., Ansari, M. and Safiey, A. (2018), "Evaluation of seismic performance of mid-rise reinforced concrete frames subjected to far-field and near-field ground motions", *Earthq. Struct.*, **15**(5), 453-462. https://doi.org/10.12989/eas.2018.15.5.453.

Bolisetti, C., Whittaker, A.S. and Coleman, J.L. (2018), "Linear and nonlinear soil-structure interaction analysis of buildings and safety-related nuclear structures", *Soil Dyn. Earthq. Eng*., **107**, 218-233. https://doi.org/10.1016/j.soildyn.2018.01.026.

Borgo, M.C., Gil, I.B. and Pagan, H.L. (2006), "Strategy for the rehabilitation of R/C T beam bridges with carbon fiber reinforced polymer sheets", *Fourth LACCEI International Latin American and Caribbean Conference for Engineering and Technology (LACCET'2006)*, Mayagüez, Puerto Rico, June.

Borjigin, S., Kim, C.W., Chang, K.C. and Sugiura, K. (2018), "Nonlinear dynamic response analysis of vehicle–bridge interactive system under strong earthquakes", *Eng. Struct*., **176**, 500-521. https://doi.org/10.1016/j.engstruct.2018.09.014.

Brincker, R., Andersen, P. and Jacobsen, N.J. (2007), "Automated frequency domain decomposition for operational modal analysis", *Proc. of IMAC-XXIV : A Conference & Exposition on Structural Dynamics*, Orlando, Florida, USA. January.

Cai, C., He, Q., Zhu, S., Zhai, W. and Wang, M. (2019), "Dynamic interaction of suspension-type monorail vehicle and bridge: Numerical simulation and experiment", *Mech. Syst. Signal Pr.,* **118**, 388-407. https://doi.org/10.1016/j.ymssp.2018.08.062.

Catbas, F.N., Grimmelsman, K.A., Ciloglu, S.K., Burgos-Gil, I. and Coll-Borgo, M. (2006), "Static and dynamic testing of a concrete T-beam bridge before and after carbon fiber reinforced polymers (CFRP) retrofit", *J. Transport. Res. Board*, **1976**(1), 77-87. https://doi.org/10.1177/0361198106197600109

Farahani, E.M. and Maalek, S. (2017), "An investigation of the seismic behavior of a deck-type reinforced concrete arch bridge", *Earthq. Eng. Eng. Vib*., **16**, 609-625. https://doi.10.1007/s11803-017-0405-x.

Ge, J., Sahdi, M.S. and Varela, S. (2019), "Computational studies on the seismic response of the State Route 99 bridge in Seattle with SMA/ECC plastic hinges", *Front. Struct. Civil Eng*., **13**(1), 149-164. https://doi.org/10.1007/s11709-018-0482-6.

Güllü, H. and Karabekmez, M. (2017), "Effect of near-fault and far-fault earthquakes on a historical masonry mosque through 3D dynamic soil-structure interaction", *Eng. Struct*., **152**, 465-492. https://doi.org/10.1016/j.engstruct.2017.09.031.

Han, Q., Chen, J.Y., Du, X.L. and Huang, C. (2017), "Nonlinear seismic response of skewed highway bridges subjected to bidirectional near-fault ground motions", *J. Bridge Eng*., **22**(7), https://doi.org/10.1061/(ASCE)BE.1943-5592.0001052.

Harris, N.K., Obrien, E.J. and Gonzalez, A. (2007), "Reduction of bridge dynamic amplification through adjusment of vehicle suspension damping", *J. Sound Vib*., **302**, 471-485. https://doi.org/10.1016/j.jsv.2006.11.020.

Jiang, L., Kang, X., Li, C. and Shao, G. (2019), "Earthquake response of continuous girder bridge for high-speed railway: A shaking table test study", *Eng. Struct*., **180**, 249-263. https://doi.org/10.1016/j.engstruct.2018.11.047.

Jo, J.S., Jung, H.J. and Kim, H. (2008), "Finite element analysis of vehicle–bridge interaction by an iterative method", *Struct. Eng. Mech*., **30**(2), 165-176. http://doi.org/10.12989/sem.2008.30.2.165.

Kameshwar, S. and Padgett, J.E. (2018), "Effect of vehicle bridge interaction on seismic response and fragility of bridges", *Earthq. Eng. Struct. Dyn*., **47**(3), 697-713. https://doi.org/10.1002/eqe.2986.

Kim, C. and Ro, P.I. (2002), "An accurate full car ride model using model reducing techniques", *J. Mech. Des*., **124**, 697-705. https://doi.org/10.1115/1.1503065.

Li, Y. and Conte, J.P. (2016), "Effects of seismic isolation on the seismic response of a California high-speed rail prototype bridge with soil-structure and track-structure interactions", *Earthq. Eng. Struct. Dyn*., **45**, 2415-2434. https://doi.org/10.1002/eqe.2770.

Liao, W.I., Loh, C.H. and Le, B.H. (2004), "Comparison of dynamic response of isolated and non-isolated continuous girder bridges subjected to near-fault ground motions", *Eng. Struct*., **26**, 2173-2183. https://doi.org/10.1016/j.engstruct.2004.07.016.

Liu, K., Zhang, N., Xia, H. and De Roeck, G. (2014), "A comparison of different solution algorithms for the numerical analysis of vehicle–bridge interaction", *J. Struct. Stab. Dyn*., **14**(2), https://doi.org/10.1142/S021945541350065X.

Mottershead, J.E., Link, M. and Friswell, M. (2011), "The sensitivity method in finite element model updating: A tutorial", *Mech. Syst. Signal Pr*., **25**(7), 2275-2296. https://doi.org/10.1016/j.ymssp.2010.10.012.

Neethu, B., Das, D. and Garia, S. (2017), "Effects of ground motion frequency content on performance of isolated bridges with SSI", *Earthq. Struct*., **13**(4), 353-363. https://doi.org/10.12989/eas.2017.13.4.353.

Paraskeva, T.S., Dimitrakopoulos, E.G. and Zheng, Q. (2017), "Dynamic vehicle-bridge interaction under simultaneous vertical earthquake excitation", *Bulletin Earthq. Eng*., **15**, 71-95. https://doi.org/10.1007/s10518-016-9954-z.

Reynders, E., Teughels, A. and DeRoeck, G. (2010), "Finite element model updating and structural damage identification using OMAX data", *Mech. Syst. Signal Pr*., **24**(5), 1306-1323. https://doi.org/10.1016/j.ymssp.2010.03.014.

Simos, N., Manos, G.C. and Kozikopoulos, E. (2018), "Near- and far-field earthquake damage study of the Konitsa stone arch Bridge", *Eng. Struct*., **177**, 256–267. https://doi.org/10.1016/j.engstruct.2018.09.072

Uckan, E., Umut, Ö., Sisman, F.N., Karimzadeh, S. and Askan, A. (2018), "Seismic response of base isolated liquid storage tanks to real and simulated near fault pulse type ground motions", *Soil Dyn. Earthq. Eng*., **112**, 58-68. https://doi.org/10.1016/j.soildyn.2018.04.030.

Wang, L., Jiang, P., Hui, Z., Ma, Y., Liu, K. and Kang, X. (2016b), "Vehicle-bridge coupled vibrations in different types of cable stayed bridges", *Front. Struct. Civil Eng*., **10**(1), 81-92. https://doi.org/10.1007/s11709-015-0306-x.

Wang, L., Kang, X. and Jiang, P. (2016a), "Vibration analysis of a multi-span continuous bridge subject to complex traffic loading anf vehicle dynamic interaction", *KSCE J. Civil Eng*., **20**(1), 323-332. https://doi.org/10.1007/s12205-015-0358-4.

Yang, Y.B. and Yang, J.B. (2019), "State-of-the-art review on modal identification and damage detection of bridges by moving test vehicles", *J. Struct. Stab. Dyn*., **18**(2), https://doi.org/10.1142/S0219455418500256.

Yang, Y.B., Zhang, B., Wang, T., Xu, H. and Wu, Y. (2019), "Two-axle test vehicle for bridges: Theory and applications", *J. Mech. Sci*., **152**, 51-62. https://doi.org/10.1016/j.ijmecsci.2018.12.043.

Youcef, K., Sabiha, T., Mostafa, D., Ali, D. and Bachir, M. (2013), "Dynamic analysis of train-bridge system and riding comfort of trains with rail irregularities", *J. Mech. Sci. Technol*., **27**(4), 951-962. https://doi.org/10.1007/s12206-013-0206-8.

Zai, W., Zhaoling, H., Zhaowei, C. Ling, L. and Shengyang, Z. (2019), "Train–track–bridge dynamic interaction: A state-of the-art review", *Vehicle Syst. Dyn: J. Vehicle Mech. Mobil*., **57**(7), 984-1027. https://doi.org/10.1080/00423114.2019.1605085.

Zhan, Y. and Au, F.T.K. (2019), "Bridge surface roughness identification based on vehicle–bridge interaction", *J. Struct. Stab. Dyn*., **19**(7), https://doi.org/10.1142/S021945541950069X.

Zhang, N. and Xia, H. (2013), "Dynamic analysis of coupled vehicle–bridge system based on inter-system iteration method", *Comput. Struct*., **114-115**, 26-34.

Zhang, S. and Wang, G. (2013), "Effects of near-fault and far-fault ground motions on nonlinear dynamic response and seismic damage of concrete gravity dams", *Soil Dyn. Earthq. Eng.*, **53**, 217-229. https://doi.org/10.1016/j.soildyn.2013.07.014.

Zhang, X., Wen, Z., Chen, W., Wang, X. and Zhu, Y. (2019), "Dynamic analysis of coupled-tract-bridge system subjected to debris flow impact", *Adv. Struct. Eng.*, **22**(4), 919-934. https://doi.org/10.1177/1369433218785643.

Zhou, S., Song, G., Wang, R., Ren, Z. and Wen, B. (2017), "Nonlinear dynamic analysis for coupled vehicle-bridge vibration system on nonlinear foundation", *Mech. Syst. Signal Pr.*, **87**, 259-278. https://doi.org/10.1016/j.ymssp.2016.10.025.

Zhou, Y. and Chen, S. (2018), "Full-response prediction of coupled long-span bridges and traffic systems under spatially varying seismic excitations", *J. Bridge Eng.*, **23**(6), https://doi.org/10.1061/(ASCE)BE.1943-5592.0001226.

*KT*